



BILLY BOSHOFF is a post-doctoral fellow at the Civil Engineering Department of the University of Stellenbosch. He received his BEng (2001) and PhD (2007), both from this university. His research areas are construction materials, design and application of high-performance cement-based composites, and the computational modelling of non-linear cement-based materials.

Contact details:
T 021-808-4498
F 021-808-4947
bboshoff@sun.ac.za



GIDEON VAN ZIJL is a part-time professor in Structural Engineering at the University of Stellenbosch (US), as well as a part-time research fellow at the Faculty of Architecture, Delft University of Technology (TUD), The Netherlands. He obtained a BEng and MEng (1990) at the US and a PhD

(2000) in Civil Engineering at the TUD. His research interests are construction materials, including design as well as physical and computational modelling of advanced cement-based materials. Concurrently, structural design guidelines and standards for existing and new cement-based construction materials are developed in his research group at the US.

Contact details:
T 021-808-4498
F 021-808-4947
gvanzijl@sun.ac.za

A computational model for strain-hardening fibre-reinforced cement-based composites

W P Boshoff and G P A G van Zijl

The development of a computational model based on a computational continuum damage formulation for a class of strain-hardening fibre-reinforced cement-based composites (SHCC) is reported on. Particular features of SHCC mechanical behaviour, namely multiple cracking at increasing stress levels with successive cracking, and eventual failure at a single crack, require incorporation of strain-hardening and strain-softening beyond threshold levels of damage evolution. A localisation zone length scale is incorporated, related to the physical failure phenomenon of fibre pull-out in the final failure crack in SHCC. Thereby, the computational solution is regularised, causing it to become finite element mesh size-independent. A novel equivalent strain criterion is formulated, whereby the predominantly tensile (mode 1)-dominated damage formulation is improved to also capture shear-dominated (mode 2) failure with reasonable accuracy. The model is verified by finite element analysis of flexural and shear laboratory experiments performed at the Institute for Structural Engineering, University of Stellenbosch.

INTRODUCTION

Through decades of research and development, sophisticated computational models have been proposed and implemented for the structural analysis of various construction materials, including concrete. The motivation for such models is not for day-to-day design of civil engineering structures, but for use by specialists to analyse structural behaviour accurately. As a complementary tool to physical laboratory experiments, computational modelling enables the development of insight towards design guidelines. Before generalisation and simplification can be done to establish such design guidelines, full insight into, as well as quantification of structural behaviour, subjected to various actions, is required. This motivates the development of a computational model for strain-hardening fibre-reinforced cement-based composites (SHCC), a new class of cement-based material, for which existing concrete constitutive models are not applicable. This paper describes a constitutive model for SHCC and its implementation in a finite element environment.

SHCC is being developed to improve the tensile properties of cement-based composites. Whereas it can generally be classified under fibre-reinforced concrete (FRC), and more particularly high-performance fibre-reinforced cement-based composites (HPFRCC), it is distinguished from these materials by its pseudo strain-hardening over a large strain range in tension. However, it has in common with FRC the main ingredient materials, namely cement, water, aggregate and fibre.

In SHCC, high tensile strength is usually not the requirement. Rather, large tensile deformation capacity without formation of wide, unsightly and durability-impairing cracks is the aim. This is achieved by finely balancing the cement-based matrix and fibre properties. In such a well-balanced composite, matrix cracks are bridged by fibres, transferring forces across the cracks without allowing significant widening and enabling the formation of more cracks at fine spacing. Each successive crack is formed at a slightly higher tensile stress level, which is the basis of strain-hardening or increased resistance upon strain increase. For manufacturing ease, but also to produce this desired strain-hardening feature, the fibres in SHCC are short (4–25 mm) and fine (10–40 µm diameter) and used in relatively low quantities, typically less than 3 % by volume. Through standard processing in terms of mixing and casting, the fibres are usually randomly distributed and randomly orientated in the cement-based matrix. In principle, various types of fibre can be used in SHCC. Polyvinyl alcohol (PVA) fibres are currently used with success in this research project.

Various approaches to computational modelling of cement-based materials exist, starting with concepts of smeared and discrete crack models in the 1960s (Ngo & Scordelis 1967; Rashid 1968). Since then, several variations in both discrete crack modelling and the smeared approach to crack modelling evolved. In discrete modelling of cracking, discontinuities are included, either initially at known locations

Keywords: computational model, concrete, fibre, strain-hardening, damage

of eventual cracking, or as a result of mesh re-generation once such area is identified from the stress or strain field in a continuum analysis. Important developments in discrete modelling include the fictitious crack model (Hillerborg *et al* 1982), whereby modelling of fracture energy dissipation during crack propagation became objective with regard to the finite element size, that is, independent of the finite element size used. Not requiring pre-knowledge of the location of cracks, or the computationally intense re-meshing strategies, the continuum description of cracking has received intense research effort. Analogous to the mesh-independent energy dissipation by the fictitious crack model, the crack band model was proposed by Bažant and Oh (1983) and implemented in smeared crack models, eg Rots (1988), to regularise the continuum description of strain localisation, or cracking.

Alternative approaches to continuum modelling of quasi-brittle cement-based materials have evolved. Inspired by the work of Kachanov (1958), continuum damage formulations were derived by consideration of micro-cracking and volume averaging of thermodynamical formulations of these micro-structural processes and the introduction of internal variables to account for the irreversible processes. On the other hand, computational continuum plasticity formulations arose, based on the volume-averaging of micro-structural dislocations and crystalline slip. These are the underlying mechanisms of ductile behaviour such as in metals, as opposed to micro-cracking and nucleation accompanying quasi-brittle failure. However, cement-based composites are quasi-brittle materials, which have residual plastic deformations as well as damage due to micro-cracking. To generalise the damage theory to include plastic strains, the theory of coupled elasto-plasticity and damage has been developed, eg by Ortiz (1985), Lemaitre (1985) and others. Implementations of such models, however, are scarce, while constitutive laws based on continuum plasticity have been implemented and employed with reasonable success to model cracking in unreinforced concrete (Feenstra 1993; De Borst *et al* 1994) and unreinforced masonry (Lourenço 1996). Later developments of weak and strong embedded discontinuities (eg Wells & Sluys 2000) to capture localisation within continuum elements have evolved, but unconventional requirements still prevent practical implementation in general computational software packages intended for large-scale analysis.

In this paper, a continuum approach is chosen for modelling SHCC to enable large-scale analysis. A computational damage model is developed, which captures the strain-hardening and eventual strain-

softening of SHCC. Regularisation of the softening process is addressed by considering the physical length scale of localisation in SHCC, which is roughly half the fibre length. The model is characterised by mode 1 behaviour, as obtained from direct tension test results, because the failure in SHCC is dominated by crack formation. A novel consideration of mode 2 (shear) failure is introduced in the generalisation from uniaxial test response to generalised stress conditions. Subsequently, the ability of the model to simulate physical behaviour under generalised stress and strain fields is verified by the analysis of bending tests as well as shear tests (Shang & Van Zijl 2007) performed at the Institute for Structural Engineering (ISE) of the University of Stellenbosch.

COMPUTATIONAL STRATEGY/ FRAMEWORK

Computational continuum damage mechanics

The constitutive law for a linear elastic continuum can be formulated as:

$$\dot{\boldsymbol{\sigma}} = \mathbf{D}^e \dot{\boldsymbol{\varepsilon}} \quad (1)$$

Note that the overhead dot denotes the time derivative of the respective field variables. The stress and strain rate vectors, and the elastic stiffness matrix considered in plane stress are:

$$\dot{\boldsymbol{\sigma}} = \begin{Bmatrix} \dot{\sigma}_x \\ \dot{\sigma}_y \\ \dot{\tau} \end{Bmatrix}, \quad \dot{\boldsymbol{\varepsilon}} = \begin{Bmatrix} \dot{\varepsilon}_x \\ \dot{\varepsilon}_y \\ \dot{\gamma} \end{Bmatrix},$$

$$\mathbf{D}^e = \frac{E}{1-\nu^2} \begin{bmatrix} 1 & \nu & 0 \\ \nu & 1 & 0 \\ 0 & 0 & (1-\nu)/2 \end{bmatrix} \quad (2)$$

with E the elastic modulus and ν Poisson's ratio. The damage approach is based on the reduction of the material stiffness once damage occurs. This is done computationally by introducing a damage indicator ω , with value ranging from 0 (no damage) to 1 (total damage), into equation 1 as follows:

$$\dot{\boldsymbol{\sigma}} = (1-\omega)\mathbf{D}^e \dot{\boldsymbol{\varepsilon}} - \dot{\omega}\mathbf{D}^e \boldsymbol{\varepsilon} \quad (3)$$

The expression of the constitutive law in rate form in equations 1-3 makes provision for the incorporation of sources of non-linearity. Clearly the goal is to consider the non-linear mechanical response during multiple crack formation and eventual failure at a single crack in SHCC. However, in the quasi-linear damage approach the constitutive law need not be expressed in rate form as in equation 3, but the rate form allows the incorporation of other sources of non-linearities, for instance sources of time dependence. By implementing the constitu-

tive law in rate form in this project, provision is made for the introduction of shrinkage and creep, which is currently in process.

Damage evolution

Damage is considered to initiate once a threshold strain level is exceeded. In SHCC, the dominating source of non-linearity is cracking, so the threshold strain is a positive, tensile equivalent strain value defined as $\tilde{\varepsilon}_0$. An equivalent strain is required to represent a generalised strain state, to enable evaluation of damage. Once this threshold is breached, damage accumulates, described by a damage loading function as:

$$f(\tilde{\boldsymbol{\varepsilon}}) = \tilde{\boldsymbol{\varepsilon}} - \tilde{\boldsymbol{\varepsilon}}_H \quad (4)$$

with $\tilde{\boldsymbol{\varepsilon}}_H$ a scalar equivalent strain history variable which represents the largest equivalent strain achieved up to the current point in time. The so-called Kuhn Tucker loading-unloading conditions apply.

$$f \leq 0, \quad \dot{\tilde{\boldsymbol{\varepsilon}}} \geq 0, \quad f \dot{\tilde{\boldsymbol{\varepsilon}}} = 0 \quad (5)$$

This means that if the previously largest equivalent strain level is exceeded, that is, the damage loading function (equation 4) is positive, the damage level increases, and the history parameter $\tilde{\boldsymbol{\varepsilon}}_H$ is updated to the new, increased level to ensure that the damage loading function rate remains non-positive. If the function 4 is negative at a material point, unloading occurs at that point and the damage variable remains unchanged, that is, the state of damage at the material point does not increase. Note, however, that the state of damage cannot decrease, as it is considered irreversible.

The stress level depends on the strain and damage level, as given by equation 3. When loading occurs beyond the threshold strain, the stress is found as a function of the changing, current equivalent strain. Considering equation 3 in one dimension for simplicity, the damage variable becomes:

$$\omega = 1 - \frac{\sigma}{E\tilde{\varepsilon}} \quad (6)$$

with E the elastic modulus of the virgin material. This damage index is related to the uniaxial tensile behaviour of SHCC, as schematised in figure 1. Note that for general multi-stress situations, the uniaxial tensile strain in the direct tensile test is now replaced by the equivalent strain. Note also that the typical pseudo strain-hardening tensile response is simplified and represented by a tri-linear stress-strain relation, as shown in figure 1. The damage index variable ω can now be solved directly from equation 6 and the equations for the linear strain-hardening and softening. This leads to expressions for strain-hardening:

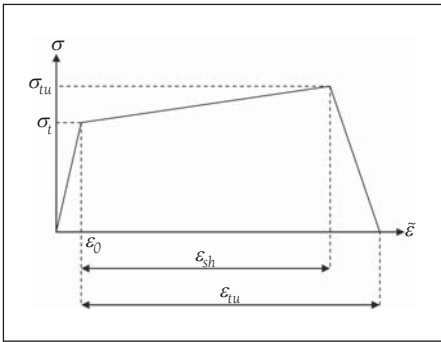


Figure 1 Tri-linear representation of the tensile response of the material

$$(\varepsilon_0 \leq \tilde{\varepsilon} < \varepsilon_0 + \varepsilon_{sh}):$$

$$\omega = 1 - \frac{\sigma_{tu} - \sigma_t}{E \varepsilon_{sh}} + \frac{\varepsilon_0 (\sigma_{tu} - \sigma_t) - \sigma_t \varepsilon_{sh}}{E \varepsilon_{sh}} \tilde{\varepsilon}^{-1} \quad (7)$$

$$\omega' = \frac{\sigma_t \varepsilon_{sh} - \varepsilon_0 (\sigma_{tu} - \sigma_t)}{E \varepsilon_{sh}} \tilde{\varepsilon}^{-2} \quad (8)$$

and for strain-softening:

$$(\varepsilon_{sh} + \varepsilon_0 \leq \tilde{\varepsilon} < \varepsilon_{tu} + \varepsilon_0):$$

$$\omega = 1 + \frac{\sigma_{tu}}{E(\varepsilon_{tu} - \varepsilon_{sh})} - \frac{\sigma_{tu}(\varepsilon_{tu} + \varepsilon_0)}{E(\varepsilon_{tu} - \varepsilon_{sh})} \tilde{\varepsilon}^{-1} \quad (9)$$

$$\omega' = \frac{\sigma_{tu}(\varepsilon_{tu} + \varepsilon_0)}{E(\varepsilon_{tu} - \varepsilon_{sh})} \tilde{\varepsilon}^{-2} \quad (10)$$

The derivatives of the damage index with regard to equivalent strain ($\omega' = \frac{\partial \omega}{\partial \tilde{\varepsilon}}$) for the respective hardening and softening regimes are also given in equations 8 and 10. They complete the constitutive description in a non-linear finite element implementation and are used to define a tangent modulus consistent with the constitutive model for efficient, quadratic converging solution strategies for the non-linear global response with regular Newton Raphson solution methods, as well as arclength methods. This constitutive model has been implemented by the first author in a user routine of the finite element program DIANA (2002).

Equivalent strain definition

For tensile-dominated boundary value problems it makes sense to relate the equivalent strain directly to the maximum principal strain. This means that damage is considered to evolve in the direction of the maximum principal tensile strain, once the threshold strain level is exceeded. This implies a rotating crack concept, as the principal strain direction at a material point may change during loading, and an increase of strain in any direction will add to the crack width included in the total strain. For such maximum principal strain damage evolution, the equivalent strain can be expressed in matrix notation as follows:

$$\tilde{\varepsilon} = \varepsilon_1 = \sqrt{\frac{1}{2} \varepsilon^T \mathbf{P}_T \varepsilon + \frac{1}{2} \mathbf{Q}^T \varepsilon} \quad (11)$$

with

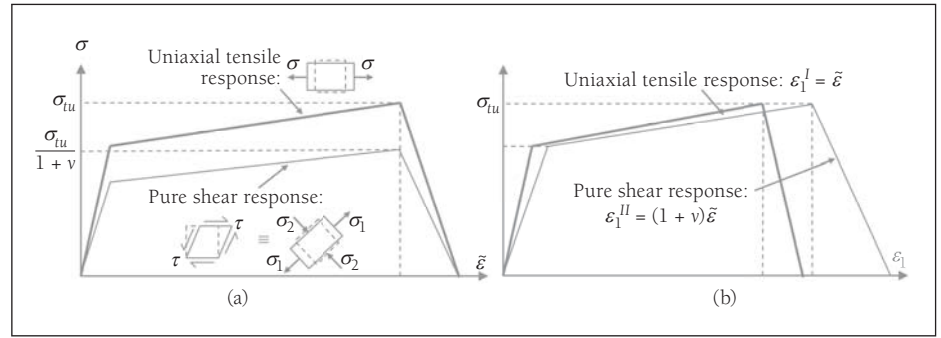


Figure 2 Tensile and pure shear responses for (a) $\tilde{\varepsilon} = \varepsilon_1$ and (b) $\tilde{\varepsilon} = \frac{\varepsilon_1 + v\varepsilon_2}{1 - v^2}$

$$\mathbf{P}_T = \frac{1}{2} \begin{bmatrix} 1 & -1 & 0 \\ -1 & 1 & 0 \\ 0 & 0 & 1 \end{bmatrix} \quad (12)$$

$$\mathbf{Q} = \begin{bmatrix} 1 \\ 1 \\ 0 \end{bmatrix} \quad (13)$$

With this formulation the computed uniaxial tensile response, referred to as mode 1 response, is exactly the same as the prescribed constitutive law shown in figure 1. However, for the case of pure shear, referred to as mode 2, which is equivalent to diagonal tension-compression, a reduced resistance is computed. These two responses are compared in figure 2. By simple stress analysis of the two boundary value problems, the stress limit ratio for a given principal strain value is given by the ratio:

$$\frac{\sigma_1^{\text{II}}}{\sigma_1^{\text{I}}} = \frac{1}{1 + \nu} \quad (14)$$

where ν is the Poisson's ratio. For high values applicable for SHCC in the order of $0,3 < \nu < 0,35$ a significantly reduced resistance in shear is computed by equation 14. For this reason, a modification of the equivalent strain formulation (equation 11) is proposed to read:

$$\tilde{\varepsilon} = \frac{\varepsilon_1 + \nu \varepsilon_2}{1 - \nu^2} = \frac{1}{(1 + \nu)} \sqrt{\frac{1}{2} \varepsilon^T \mathbf{P}_T \varepsilon} + \frac{1}{2(1 - \nu)} \mathbf{Q}^T \varepsilon \quad (15)$$

With this formulation the uniaxial tensile response is left unaltered, and the pure shear response is now equal to the uniaxial tensile response in $\sigma_1 - \tilde{\varepsilon}$ space. However, in the $\sigma_1 - \varepsilon_1$ space a larger deformability is computed for the pure shear case, as shown in figure 2b.

Regularisation of the softening response

The requirement of regularisation of the continuum description of softening processes is well-known. If it is not done, the size of the element chosen for a finite element analysis will influence the response, resulting in less energy dissipation upon use of a smaller element size. In the crack band

method (Bažant & Oh 1983, Rots 1988) the element size is related to the crack band width in which localisation and associated softening takes place. Several other regularisation techniques have been proposed that extend the equivalent stress or strain formulations to incorporate non-local strain considerations (Pijaudier-Cabot & Bažant 1987) and strain gradients (Peerlings *et al* 1998), or strain rate (Sluys 1992, Van Zijl *et al* 2001).

In the current formulation, a local material length scale (L_m) equal to half the fibre length (L_f) is considered:

$$L_m = \frac{L_f}{2} \quad (16)$$

This is related to the phenomenon of fibre pull-out from the matrix in the final failure crack in ECC. Hereby, the failure crack opening to a width of $L_f / 2$ coincides with the point of complete loss of resistance. In the implementation of the model, to prevent element size dependence of the energy dissipation, the softening strain (ε_s) branch is expressed as a softening length, normalised by the element size (L_e) as follows:

$$\varepsilon_s = \frac{L_m}{L_e} \quad (17)$$

This results in a smaller softening strain for larger elements and vice versa, whereby the softening deformational response is independent of the element size. For materials as ductile as SHCC, it is often found that a local softening is initially spread over a region, that is, local loss of strength occurs at several of the micro-cracks due to their widening. Only at a later stage localisation occurs in a single failure crack. This means that an initial voluminous softening is followed by a localised softening. In FE analysis of SHCC this is simulated by a spread-out region of elements entering softening, before localised softening into a single row, column or diagonal selection of elements. In this scenario the abrupt introduction of the length scale leads to element size-dependent, excessive energy dissipation, due to the initial spread-out nature of

Table 1 Ingredients and mass ratios of SHCC bending specimens

Cement (CEM I 42.5)	Fly ash	Corex slag	Water	Sand	Fibre V _f (%)	Number of specimens	
						Tensile	Bending
0,4	0,5	0,1	0,4	0,5	2,0	7	6

Table 2 Model parameters from tensile tests, used for 3-point bending analysis

	Elastic modulus (MPa)	Poisson's ratio	σ _t (MPa)	σ _{tu} (MPa)	ε _{sh} (%)	L _f /2 (mm)
Average	9 100	0,35	2,23	2,8	3,9	6
Coefficient of variation	12,6 %	-	2,8 %	9,2 %	19,5%	-

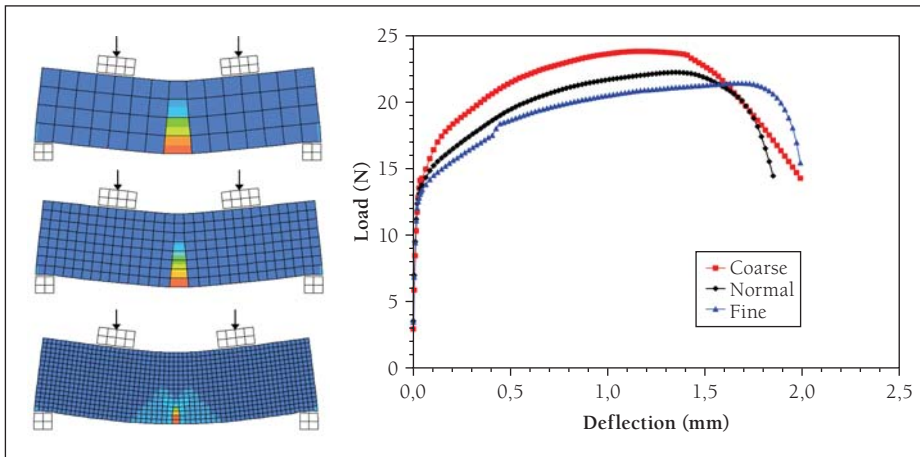


Figure 3 Mesh objectivity in four-point bending

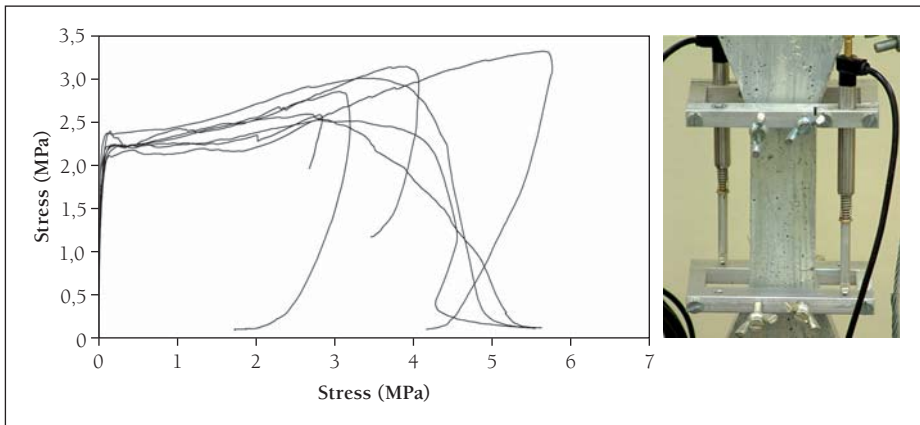


Figure 4 Direct, uniaxial tensile test result for model parameter determination

softening. Therefore, a hybrid formulation is adopted.

Global and local softening approach

Motivated by the observation of widening of several cracks, but eventual localisation in a single failure crack, the concepts of global softening ε_{sG} and local softening ε_{sL} are introduced. The local softening strain follows the standard crack band approach, replacing equation 17 as follows:

$$\epsilon_{sL} = \frac{L_m}{L_e} \tag{18}$$

For the global softening formulation, consider the number of cracks entering softening:

$$n_s = \frac{L_e}{S} \tag{19}$$

with S the spacing of these softening cracks. With the assumption of average crack width in an element, the global softening strain can then be expressed as

$$\epsilon_{sG} = n_s \epsilon_{sL} = \frac{L_e}{S} \frac{L_m}{L_e} = \frac{L_m}{S} \tag{20}$$

Note that the boundary value problem and the material ductility determine crack spacing and the eventual localising crack. It is essential that all elements entering softening utilise the global strain localisation definition, but that only the failure crack subsequently experiences local softening strain, as expressed by equation 18. For generalisation in FE implementation, a weighted combination is used to express the total softening strain in an element:

$$\epsilon_s = \alpha \epsilon_{sG} + (1 - \alpha) \epsilon_{sL} \tag{21}$$

The factor α weighs the amount of global softening in an element, which is typically set to the value of 0,7 in combination with the spacing S = 6 mm. These values are based on observations of localising crack spacing and inverse analysis. The mesh objectivity is demonstrated in a numerical analysis of four-point bending, shown in figure 3. The same geometry is modelled with increasing mesh density, using linearly interpolated quadrilateral elements. The flexural response, shown in figure 3 (right), converges with increasing mesh density, or reducing element size, with reasonable agreement in the computed responses for the finer two meshes shown on the left. Contours of maximum principal strain are shown on the deformed beams on the left, indicating the localisation in the central crack.

EXPERIMENTAL STUDIES

Three-point bending

SHCC beams were recently tested in three-point bending. This test was simulated to study the ability of the computational model for SHCC to capture structural response in more general boundary value problems.

Model parameter characterisation

The model parameters required were determined from direct uniaxial tensile tests on dog-bone shaped specimens of the same dimensions and in the same set-up as described in Shang & Van Zijl (2007). These tensile specimens were cast using the same mix proportions as the beams for the three-point bending tests, and cured in the same conditions. The mix ingredients and proportions are given in table 1. Note that poly-vinyl alcohol fibres of 12 mm in length and 40 μm in diameter, supplied by Kuraray, Japan, were used. The material was mixed in an 8 litre-capacity Hobart-type laboratory mixer, after which both the tensile and bending specimens were cast in steel moulds and kept in a moist spray room at 23 °C. They were stripped after three days and subsequently kept in water at a constant temperature of 23 °C up to the age of 14 days. At this age, the tensile specimens were tested in a Zwick Z250 materials testing machine under displacement control at 0,5 mm/minute displacement of the testing machine crosshead. The strain of the specimens was measured using HBM LVDTs over a gauge length of 80 mm, as shown in figure 4. Note that the reduction in deformation in the softening branch for some specimens indicates that the final failure crack was outside the gauge area. From the tensile results, the average model parameter values were determined, as summarised in table 2. The

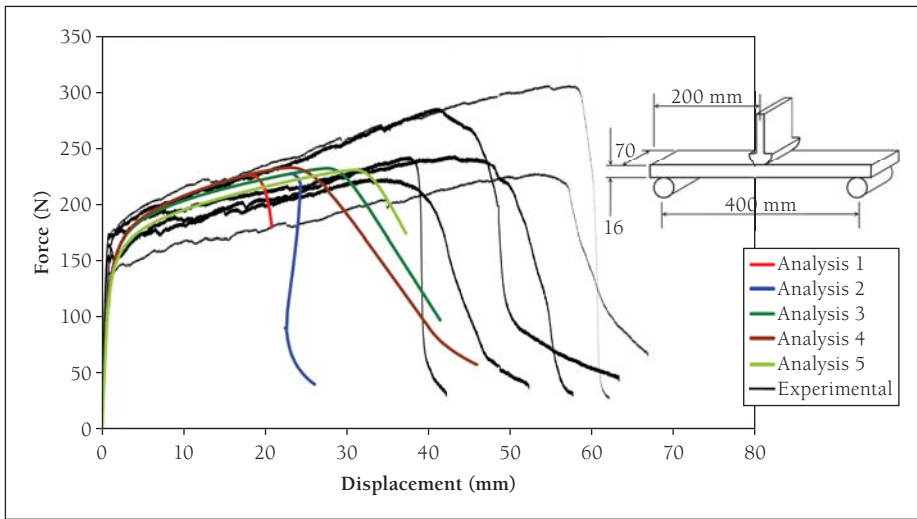


Figure 5 Three-point bending test results

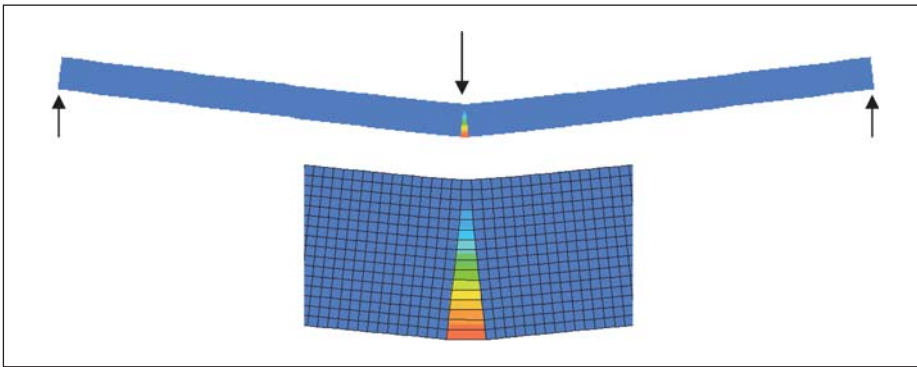


Figure 6 Mesh with contours of the maximum principal strain showing the position of the localising crack

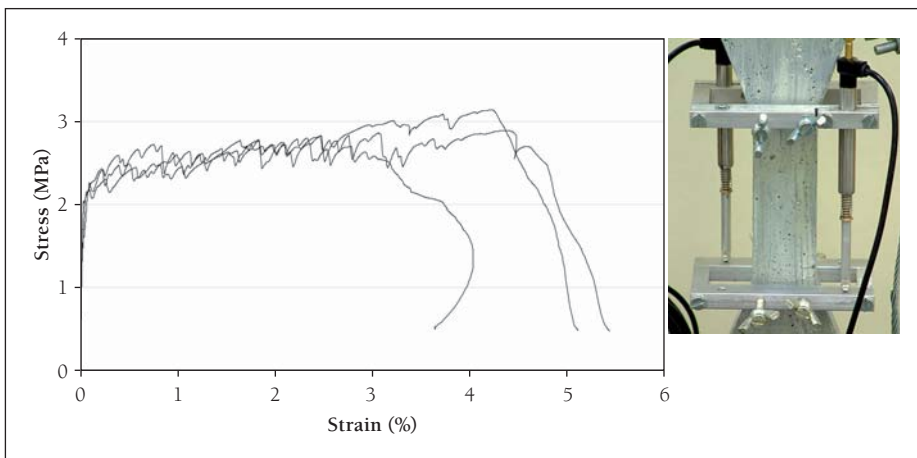


Figure 7 Direct, uniaxial tensile test result for model parameter determination

bending tests were performed at the same age as the tensile test specimens. The bending tests were performed in the same materials testing machine, under displacement control at 5,0 mm/minute displacement of the cross-head. The plate beams were of nominal dimensions, 16 mm thick, 70 mm wide and 500 mm in length, tested over a span length of 400 mm, figure 5.

Finite element model of three-point bending test

The beams were modelled in plane stress, using linearly interpolated, 4-noded plane stress elements. The element size in the localising region of the beam was chosen at 1 mm. Five analyses were done with differ-

ent parameters in a sensitivity analysis. The parameters are shown in table 3. Analyses 1 to 4 were to investigate the effect of α together with the ductility found in the tensile tests. The value of 3,9 % for the ultimate strain is the average value, and the 5,7 % is the maximum value attained in a single tensile test. For analysis 5 the first cracking stress, σ_t , was reduced to the minimum value found in a tensile test, that is 2,10 MPa.

Results

The experimental results are compared with the numerical results in figure 5. The strain distribution is shown in figure 6, where the localised crack is shown clearly.

Table 3 Model parameters from the sensitivity analyses

Analysis	σ_t (MPa)	ϵ_{sh} (%)	α
1	2,23	3,9	0,7
2	2,23	5,7	0,7
3	2,23	5,7	0
4	2,23	3,9	0
5	2,10	5,7	0

Analysis 1 was done with the average values of the corresponding tensile tests as parameters. The computed response is far less ductile than the measured responses even though the ultimate strength compares well. Even if the value of the ultimate strain is increased to the maximum value obtained in the tensile tests (analysis 2), the ductility remains relatively low. The influence of the localisation factor α is demonstrated in analyses 3–5. It is clear that an improvement in ductility is found, indicating that the physical meaning of this parameter must be studied carefully and not chosen merely for computational convenience.

A source of ductility was found in the prescribed matrix cracking stress. For lower matrix strength, a larger zone of multiple cracks is computed, adding ductility, as is clearly demonstrated by the computed responses for analyses 4 and 5. Boshoff and Van Zijl (2007) found that the first cracking stress is highly dependent on the testing speed. A difference of up to 40 % is found if the testing speed is varied over four orders of magnitude, yet still within the quasi-static range. This implies that rate effects, including creep, may hold the key to the large observed ductility in bending. The introduction of time dependence into the model is currently being undertaken.

Shear test

To study the ability of the model to capture shear-dominated failure, the Iosipescu shear tests on SHCC specimen type S4, reported in detail in the paper (Shang & Van Zijl 2007) on page 16, were analysed.

Model parameter characterisation

The model parameters required are shown in figure 1. They are determined from direct uniaxial tensile tests on dog-bone shaped specimens as described in Shang & Van Zijl (2007). Care was taken to prepare the tensile specimens from the same mix and in the same manner as the shear specimens, for parameter characterisation purposes. The binder composition of the mix differed slightly from the mix in the previous experimental study. The mix proportions are given in table 4. The resulting tensile responses of the S4 specimens (Shang & Van Zijl 2007) are shown in figure 7. From these results of three dog-bone specimens, the average

Table 4 Ingredients and mass ratios of SHCC shear specimens

Cement (CEM I 42.5)	Fly ash	Corex slag	Water	Sand	Fibre V_f (%)	Number of specimens
0,5	0,45	0,05	0,4	0,5	2,0	3

Table 5 Model parameters from tensile tests, used for SHCC losipescu shear analysis

	Elastic modulus (MPa)	Poisson's ratio (ν)	σ_t (MPa)	σ_{tu} (MPa)	ϵ_{sh} (%)	$L_f/2$ (mm)
Average	8 520	0,35	1,85	2,92	3,51	6
Coefficient of variation	16 %	-	9 %	7 %	31 %	-

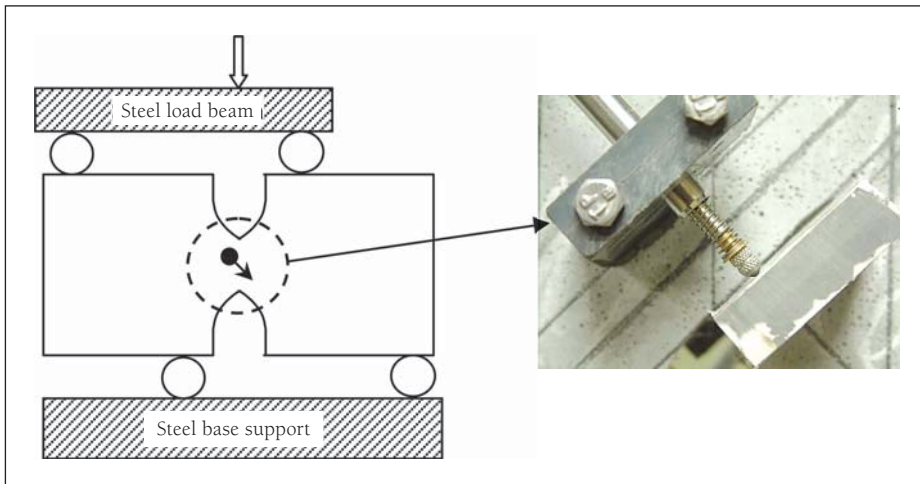


Figure 8 Finite element model and boundary values for losipescu shear test

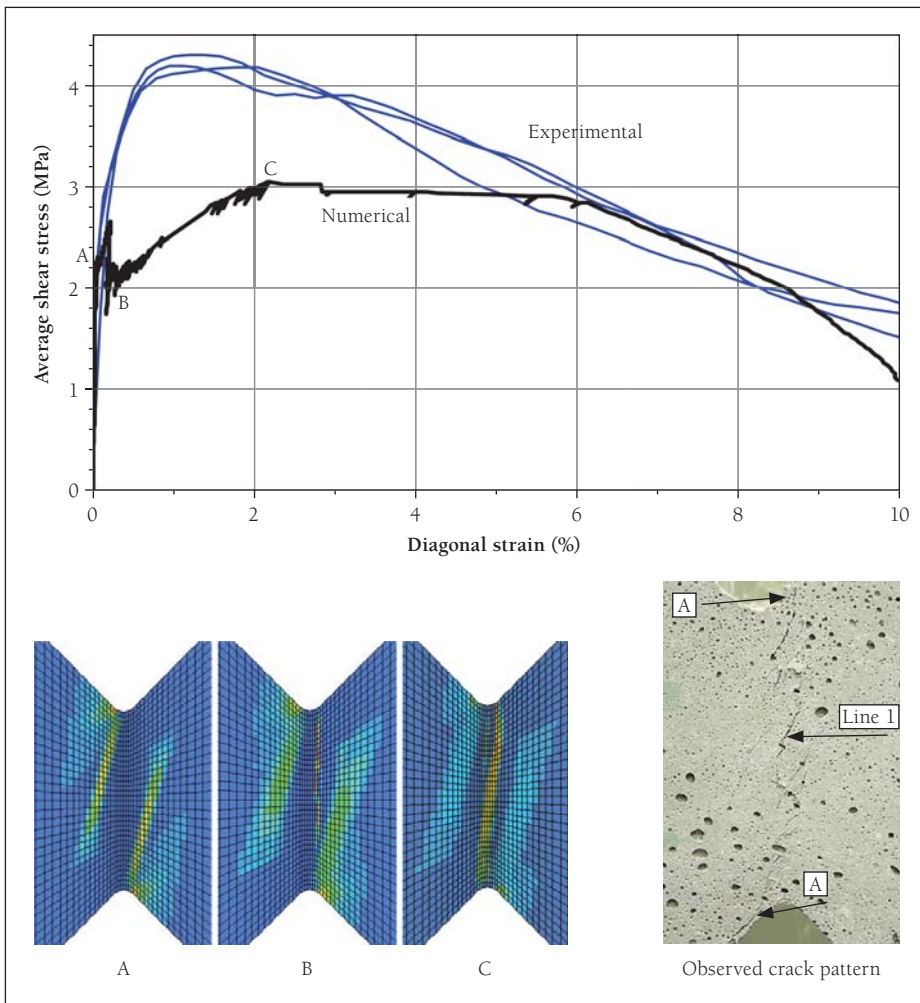


Figure 9 Measured and computed responses to losipescu shear testing of SHCC, also showing principal strain contours at various stages (A-D)

values were determined, as summarised in table 5.

Finite element model of losipescu shear test

The losipescu specimen of geometry given by Shang & Van Zijl (2007) was modelled in plane stress, using linearly interpolated, 4-noded plane stress quadrilateral elements. The load transfer and supports in the experimental set-up, shown in figure 8, were simulated with point loads at the upper cylindrical bearing loads and point supports at the lower cylinders for simplicity. For comparison with the diagonal tensile deformation LVDT measurements during the experiments, the relative displacement of two nodes placed appropriately at the ends of the LVDT gauge length, was monitored in the FE analysis. From these relative displacements, the average strain over the original diagonal length of 25 mm was computed.

Results

In figure 9 the computed average diagonal strain over the 25 mm gauge length is compared with the experimental responses of the shear specimens. The average shear stresses were computed by the internal shear force at the notch at a particular loading point in time, divided by the total sectional area between the notch apexes.

Also shown in the figure are contours of maximum principal strain in the notch area, at three stages of the shear test, namely the first peak (A), at the bottom after the first peak (B), and at the maximum computed resistance. In the early stages (A), localisation arises at a different orientation, but this is arrested and a new localisation band initiates in the notch area (B) and propagates in the alignment until peak load (C). This is in reasonable agreement with the observed localisation patterns in the ultimate stage.

By the choice of the equivalent strain definition (equation 15) for damage evolution, pure shear is considered to have the same diagonal tensile resistance, but increased deformability (figure 2b). This is clearly reflected in the computed losipescu shear response in figure 9, which is repeated in figure 10, where the uniaxial tensile stress-strain responses are also shown. Note that the shear stress state in the losipescu specimen is equivalent to the biaxial normal stress state of diagonal tension and orthogonal compression. It should thus be kept in mind that the shear response in figure 10 includes the confining orthogonal compression, while the direct tensile response does not benefit from such confining pressure. Clearly, enhanced resistance, beyond pure diagonal tensile resistance, occurs in pure shear, which remains to be characterised by further losipescu tests of SHCC for identification of mechanisms of shear failure.

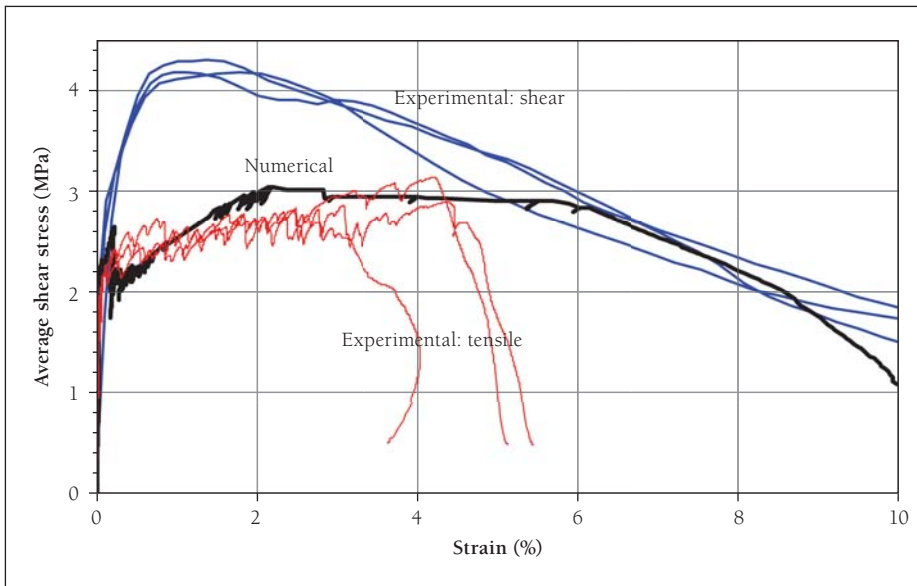


Figure 10 Measured and computed shear responses in terms of diagonal strain, also showing uniaxial tensile stress-strain responses

SUMMARY AND CONCLUSION

A numerical model for SHCC has been motivated and elaborated on. Its ability to capture several phenomena in mode 1-dominated failure in tension and bending, but also mode 2 shear response of these materials, was studied by the analysis of laboratory tests in direct tension, bending and shear. The following conclusions can be drawn:

- By using average values for the model parameters from direct tensile tests on SHCC, the computed
 - load which causes first cracking
 - subsequent strain-hardening gradient, and the
 - peak load
 in bending are in reasonable agreement with the averages of the corresponding measured values.
- A significantly lower ultimate deflection in the bending test is computed than measured in the experiments. By altering model parameters that increase the size of the flexural cracking zone, increased ultimate ductility is computed. The model parameters that have this effect are the first cracking stress σ_t and the global softening parameter α . A lower value for σ_t causes a larger area where cracks initiate, while a lower value for α increases the softening strain assigned to a single element, leading to increased ductility. The mechanisms of high bending ductility must be studied further to improve the prediction capacity of the model.
- The computed shear strength of SHCC underestimates the measured shear strength by 30%. This is due to the increased tensile capacity under biaxial/shear conditions which is not captured by the current model implementation. To enable accurate prediction of mode 2-type (shear) strength, more experimental characterisation of shear behaviour, and/or behaviour under biaxial loading is required.

ACKNOWLEDGEMENT

The support of the Department of Trade and Industry through the Technology and Human Resources for Industry Programme (THRIP), as well as the industrial partners of the THRIP project 2660, APERC Structures, is gratefully acknowledged. Several past and present graduate and post-graduate students have contributed to this concrete materials-related research since 2002. Their contributions are invaluable as are their continued sound application of the knowledge and insight developed during their research.

REFERENCES

- Bazant, Z P and Oh, B H 1983. Crack band theory for fracture of concrete. *Materials and Structures*, 16(93):155–177.
- Boshoff, W P and Van Zijl, G P A G 2006. Time-dependent response of ECC: Characterisation and modelling of creep and creep fracture, submitted to *Cement and Concrete Research*.
- De Borst, R, Feenstra, P H, Pamin, J and Sluys, L J 1994. Some current issues in computational mechanics of concrete. In H Mang *et al* (eds), *Computational modelling of concrete structures*. Swansea: Pineridge Press, pp 283–302.
- DIANA 2002. *Diana Finite Element Analysis User's Manual*, release 8.1, TNO Building, The Netherlands.
- Feenstra, P H 1993. Computational aspects of biaxial stress in plain and reinforced concrete. Dissertation, Delft University of Technology, Delft, The Netherlands.
- Hillerborg, A, ModYeer, M and Petersson, P E 1976. Analysis of crack formation and crack growth in concrete by means of fracture mechanics and finite elements. *Cement and Concrete Research*, 6:773–782.
- Kachanov, L M 1958. On the time to failure under creep conditions (in Russian). *Izv Akad Nauk USSR Otd Tekhn Nauk*, 8:26–31.
- Lemaitre, J 1985. Coupled elasto-plasticity and damage constitutive equations. *Computational Methods in Applied Mechanics and Engineering*, 107:83–87.
- Lourenço, P B 1996. Computational strategies for masonry structures. Dissertation, Delft University of Technology, Delft, The Netherlands.
- Ngo, D and Scordelis, A C 1967. Finite element analysis of reinforced concrete beams. *Journal of the American Concrete Institute*, 64:152–163.

- Ortiz, M 1985. A constitutive theory for inelastic behaviour of concrete. *Mechanics of Materials*, 4:67–93.
- Peerlings, R H J, De Borst, R, Brekelmans, W A M and Geers, M G D 1998. Gradient-enhanced damage modelling of concrete fracture. *Mechanics of Cohesive Frictional Materials*, 3:323–342.
- Pijaudier-Cabot, G and Bazant, Z 1987. Nonlocal damage theory. *ASCE Journal of Engineering Mechanics*, 113(10):1512–1533.
- Shang, Qinjiang and Van Zijl, G P A G 2007. Characterising the shear behaviour of strain-hardening fibre-reinforced cement-based composites. *Journal of the South African Institution of Civil Engineering*, 49(2):16–23.
- Rashid, Y R 1968. Analysis of prestressed concrete pressure vessels. *Nuclear Engineering*, 7:334–344.
- Rots, J G 1988. Computational modeling of concrete fracture. Dissertation, Delft University of Technology, Delft, The Netherlands.
- Van Zijl, G P A G, De Borst, R and Rots, J G 2001. The role of crack rate dependence in the long term behaviour of cementitious materials. *International Journal of Solids and Structures*, 38:5063–5079.
- Wells, G N, Sluys, L J 2000. Application of embedded discontinuities for softening solids. *Engineering Fracture Mechanics*, 65:263–281.

LIST OF SYMBOLS

- α Material model parameter for portion of global softening
- \mathbf{D}^e Elastic stiffness matrix
- E Elastic modulus of virgin material
- $\boldsymbol{\varepsilon}$ Strain vector
- $\boldsymbol{\varepsilon}_x$ Normal stress in x-direction
- $\boldsymbol{\varepsilon}_y$ Normal strain in y-direction
- $\boldsymbol{\varepsilon}_0$ Elastic strain limit
- $\boldsymbol{\varepsilon}_{sh}$ Tensile strain-hardening range
- $\boldsymbol{\varepsilon}_s$ Softening strain
- $\boldsymbol{\varepsilon}_{sL}$ Localised softening strain
- $\boldsymbol{\varepsilon}_{sG}$ Global softening strain
- $\boldsymbol{\varepsilon}_{if}$ Tensile strain-hardening + softening range
- $\boldsymbol{\varepsilon}_{tu}$ Inelastic ultimate strain
- $\tilde{\boldsymbol{\varepsilon}}$ Equivalent strain
- $\tilde{\boldsymbol{\varepsilon}}_0$ Equivalent strain threshold
- $\tilde{\boldsymbol{\varepsilon}}_H$ Equivalent strain history variable
- $\boldsymbol{\varepsilon}_1$ Algebraic maximum principal strain
- $\boldsymbol{\varepsilon}_2$ Algebraic minimum principal strain
- $\boldsymbol{\varepsilon}_1^I$ Maximum principal strain for type 1 loading (direct tension)
- $\boldsymbol{\varepsilon}_1^{II}$ Maximum principal strain for type 2 loading (direct shear)
- γ Shear strain
- f Damage loading function
- L_e Finite element size
- L_f Fibre length
- L_m Material length scale
- n_s Number of cracks entering softening
- \mathbf{P}_T Principal strain projection matrix
- $\boldsymbol{\pi}$ Principal strain projection vector

S	Material model parameter for the crack spacing	σ_x	Normal stress in x-direction	σ_1^II	Maximum principal stress for type 2 loading (direct shear)
σ	Stress vector	σ_y	Normal stress in y-direction	τ	Shear stress
σ_t	First cracking stress	σ_1	Maximum principal stress	ν	Poisson's ratio
σ_{tu}	Material model parameter for the ultimate tensile stress	σ_1^I	Maximum principal stress for type 1 loading (direct tension)	w	Damage variable